PCCP

Accepted Manuscript

This is an *Accepted Manuscript*, which has been through the Royal Society of Chemistry peer review process and has been accepted for publication.

Accepted Manuscripts are published online shortly after acceptance, before technical editing, formatting and proof reading. Using this free service, authors can make their results available to the community, in citable form, before we publish the edited article. We will replace this *Accepted Manuscript* with the edited and formatted *Advance Article* as soon as it is available.

You can find more information about *Accepted Manuscripts* in the Information for Authors.

Please note that technical editing may introduce minor changes to the text and/or graphics, which may alter content. The journal's standard Terms & Conditions and the Ethical guidelines still apply. In no event shall the Royal Society of Chemistry be held responsible for any errors or omissions in this *Accepted Manuscript* or any consequences arising from the use of any information it contains.

ROYAL SOCIETY OF CHEMISTRY

www.rsc.org/pccp

Submitted to PCCP, 11/7/2014, revised 12/9/2014

Insights into the bond-selective reaction of Cl + HOD(n_{OH}) → HCl + OD

Jun Li,[1,2,*] Hongwei Song,[2] and Hua Guo[2,*]

[1]*School of Chemistry and Chemical Engineering, Chongqing University, Chongqing 400030, China*

[2]*Department of Chemistry and Chemical Biology, University of New Mexico, Albuquerque, New Mexico 87131, USA*

*: corresponding authors, emails: jlii4@cqu.edu.cn, hguo@unm.edu

Physical Chemistry Chemical Physics Accepted Manuscript

Abstract

Bond-selective reaction dynamics of the title reaction is investigated using full-dimensional quantum dynamical (QD) and quasi-classical trajectory (QCT) methods on a newly constructed *ab initio* global potential energy surface. Both QD and QCT results indicate that excitation of the local OH vibration in the HOD reactant renders the reaction strongly bond selectivity, with the OD/OH branching ratio in quantitatively agreement with experiment. In addition, the reactivity is found to be greatly enhanced with the reactant vibrational excitation, thanks to the change of a direct rebound mechanism to a capture mechanism. The QCT calculations also yield product state distributions, which show that the HCl product is vibrationally and rotationally hot while the OD co-product is internally cold. The bond selectivity, vibrational enhancement, and product energy disposal are rationalized by the Sudden Vector Projection model.

Physical Chemistry Chemical Physics Accepted Manuscript

I. Introduction

A key objective of chemistry is to transform reactants into designed products. Hence, control of reaction pathways and product branching is of great importance. In the practical level, control can indeed be achieved nowadays by imparting energy into various reactant modes, using for example lasers.[1] Thanks to the non-statistical nature of direct reactions, some of reactant modes may have larger couplings with the reaction coordinate than others, leading to promotional effects. Indeed, such mode specificity has been demonstrated in several reactive systems.[2-3] In some cases, it is even possible to selectively break the desired chemical bond by vibrationally exciting reactant molecules.[4] Such bond selectivity is directly akin to the central goal of chemistry and provides details on the energy flow in the reactive system.[5-6] To better design future mode specific and/or bond selective chemistry, it is important to understand the dynamics at the microscopic level. In this publication, we focus on the Cl + HOD → HCl + OD reaction, the bond selective chemistry of which has been unambiguously demonstrated by exciting the O-H vibration in HOD.[7-8] Strong bond selective chemistry has also been observed in the analogous H + HOD reaction.[9-14] Both reactions have "late" barriers, underscoring the potential enhancement effects of reactant vibrational excitation, according to Polanyi's Rules.[15]

Theoretical studies of this[16-20] and the analogous H + HOD reactions[21-25] have been reported before, many with approximations. Here, we present definitive results for the title reaction. To this end, we first report a refit of the full-dimensional global potential energy surface (PES) to a large number of high-level *ab initio* points[26] using our newly proposed high-fidelity permutation invariant polynomial-neural network (PIP-NN) method.[27-28] This PIP-NN PES provides a much more accurate description of the topography of the PES governing the reaction, thus offering a much more reliable platform for dynamics than previous studies based

Physical Chemistry Chemical Physics Accepted Manuscript

on either empirical or reduced-dimensional PESs.[16-19] Second, we performed not only quasi-classical trajectory (QCT), but also full-dimensional initial state specific quantum dynamics (QD) calculations. The QD-QCT comparison permits a direct assessment of the importance of quantum effects in this hydrogen abstraction reaction. Unlike the previous reduced-dimensional models,[17-19] the full-dimensional QD model treats of all modes on an equal footing. On the other hand, the QCT calculations yield product state distributions, which can be directly compared with experimental data. Both QCT and QD studies of the Cl + H_2O → HCl + OH reaction and its mode specificity have been reported by us earlier,[26, 29] and here we focus on the bond selective aspects of the title reaction. In addition, this system also offers a testing case for the recently proposed Sudden Vector Projection (SVP) model, which attempts to predict mode specificity and bond selectivity from the coupling of reactant modes with the reaction coordinate at the transition state.[29-32] The SVP model, which has been successfully applied to many reactions,[33] can be considered as an extension of the venerable rules of Polanyi.[15] Like Polanyi's Rules, the SVP model emphasizes the paramount role of the transition state in controlling bond selectivity in chemical reactions. The paper is organized as follows. Section II outlines the QD and QCT methods and provides calculation details. The results are presented and compared with available experimental and theoretical data in Section III. These results are discussed in Section IV, followed by conclusions in Section V.

II. Theory

II.A Potential energy surface

Previously, our group developed a full-dimensional global PES for the Cl + H_2O → HCl + OH reaction based on ~25,000 points at the Davidson corrected multi-reference configuration

Physical Chemistry Chemical Physics Accepted Manuscript

interaction level with the correlation-consistent aug-cc-pVTZ basis set (MRCI+Q/AVTZ) using the permutation invariant polynomial (PIP) fitting method of Bowman and coworkers.[34] The total root mean square error (RMSE) was 34.7 meV.[26] To further reduce the fitting error, we report here a new fit of the same *ab initio* data set using our newly proposed permutation invariant polynomial-neural network (PIP-NN) method.[27-28] The non-linear nature of NNs provides a flexible means to approximate any unknown real-valued multi-dimensional function accurately.[35] The non-linear parameters defining the NN are obtained by "training" with the data set. Our PIP-NN approach[27-28] enforces permutation symmetry in the NN fitting by employing a special set of symmetry functions as the input vector, rather than the geometries themselves. The symmetry functions are PIPs of the Morse variables defined in terms of internuclear distances, as introduced by Xie and Bowman.[36] An important point in the PIP-NN fitting of PESs for systems with four or more atoms is that more PIPs than the internal coordinates are needed to ensure permutation invariance.[28]

Similarly to the much studied F + H_2O system,[28] the maximum total order of the PIPs in the input vector is two, resulting in 17 PIPs. In the NN fitting, the data were divided randomly into three sets, namely the training (90%), validation (5%), and test (5%) sets. To avoid false extrapolation due to edge points in the randomly selected validation and test sets, only fits with similar RMSEs (defined as RMSE=$\sqrt{\sum_{i=1}^{N}\left(E_{\text{output}}-E_{\text{target}}\right)^2/N}$) for all three sets were accepted. In addition, the maximum deviation was also used in selecting the final fits.

II.B Quantum dynamics

The full-dimensional Hamiltonian in the atom-triatom Jacobi coordinates, as shown in Fig. 1, for a given total angular momentum J is written as ($\hbar=1$):[37]

Physical Chemistry Chemical Physics Accepted Manuscript

$$\hat{H} = -\frac{1}{2\mu_R}\frac{\partial^2}{\partial R^2} + \hat{h}_1(r_1) + \hat{h}_2(r_2) + \frac{(\hat{J} - \hat{j}_{12})^2}{2\mu_R R^2} + \frac{\hat{l}_1^{\,2}}{2\mu_1 r_1^{\,2}} + \frac{\hat{j}_2^{\,2}}{2\mu_2 r_2^{\,2}} + \hat{V}(R, r_1, r_2, \theta_1, \theta_2, \varphi_1) - V_1^{ref}(r_1) - V_2^{ref}(r_2), \quad (1)$$

where R is the distance between the attacking atom Cl and HOD centre of mass, r_1 the distance between H and the centre of mass of OD, and r_2 the bond length of OD, with μ_R, μ_1, and μ_2 as their corresponding reduced masses. $\hat{l}_1$ is the orbital angular momentum operator of H with respect to OD and $\hat{j}_2$ is the rotational angular momentum operator of OD, which are coupled to $\hat{j}_{12}$. The one-dimensional (1D) reference Hamiltonians are defined as

$$\hat{h}_i(r_i) = -\frac{1}{2\mu_i}\frac{\partial^2}{\partial r_i^2} + V^{ref}(r_i), \qquad i = 1, 2 \quad (2)$$

where $V^{ref}(r_i)$ are the corresponding 1D reference potentials along the coordinate r_i. Non-adiabatic effects are not considered in this work.

The parity (ε) adapted wave function is expanded in terms of the body-fixed (BF) bases:

$$\psi^{JM\varepsilon}(\vec{R}, \vec{r}_1, \vec{r}_2) = \sum_{n, v_1, v_2 j, K} F^{JM\varepsilon}_{n v_1 v_2 j K} u_n^{v_1}(R) \phi_{v_1}(r_1) \phi_{v_2}(r_2) \Phi^{JM\varepsilon}_{jK}(\hat{R}, \hat{r}_1, \hat{r}_2), \quad (3)$$

where n labels the translational basis functions, v_1 and v_2 represent the vibrational basis indices for r_1 and r_2, and the composite index j denotes (l_1, j_2, j_{12}). The translational basis functions, $u_n^{v_1}$, are dependent on v_1 due to the use of an L-shaped grid.[38] $\Phi^{JM\varepsilon}_{jK}(\hat{R}, \hat{r}_1, \hat{r}_2)$ in Eq. (3) are the parity-adapted coupled BF total angular momentum eigenfunctions, which are defined as

Physical Chemistry Chemical Physics Accepted Manuscript

$$\Phi_{jK}^{JM\varepsilon} = (1+\delta_{K0})^{-1/2}\sqrt{\frac{2J+1}{8\pi}}[D_{K,M}^{J*}Y_{l_1 j_2}^{j_{12}K} + \varepsilon(-1)^{l_1+j_2+j_{12}+J} D_{-K,M}^{J*}Y_{l_1 j_2}^{j_{12}-K}], \quad (4)$$

where $D_{K,M}^{J}$ are the Wigner rotation matrices.[39] M is the projection of J on the z axis in the space-fixed (SF) frame, and K is the projection on the BF z axis that coincides with R. $Y_{l_1 j_2}^{JK}$ are defined as

$$Y_{l_1 j_2}^{JK} = \sum_m D_{Km}^{j_{12}*}(0,\theta_1,\phi)\sqrt{\frac{2l_1+1}{4\pi}}\langle j_2 m l_1 0 | j_{12} m\rangle y_{j_2 m}(\theta_2, 0) \quad (5)$$

and y_{jm} denote the spherical harmonics. Note that $\varepsilon(-1)^{l_1+j_2+j_{12}+J} = 1$ for $K = 0$ in Eq. (5).

The initial state-selected Chebyshev real wave packet (CRWP) method employed here for tetra-atomic systems is well documented in our earlier publications,[40-42] so only a brief discussion is given here. The initial wave packet $|\chi_i\rangle$ is constructed as the direct product of a Gaussian wave packet in the scattering coordinate and a specific ro-vibrational state of HOD in the BF representation:[43]

$$|\chi_i\rangle = Ne^{-(R-R_0)^2/2\delta^2}\cos(k_i R)|\upsilon_0 j_0 \tau; J\varepsilon\rangle, \quad (6)$$

where N is the normalization factor, R_0 and δ are the mean position and width of the initial Gaussian function and k_i is the mean momentum given by E_i via $k_i = \sqrt{2\mu_R E_i}$. The initial ro-vibrational wavefunction of HOD was obtained by diagonalizing the three-dimensional Hamiltonian of HOD, in which υ_0, j_0, and τ denote the initial vibrational quantum number, the initial angular momentum quantum number, and the parity of the reactant HOD, respectively.

Physical Chemistry Chemical Physics Accepted Manuscript

We focus in this work on vibrational excitations of the local-mode O-H stretch in HOD, which is labeled by the quantum number n_{OH}, namely $\upsilon_0 = (n_{OD} = 0, n_b = 0, n_{OH})$.

The wave packet is propagated using the Chebyshev propagator:[43-45]

$$|\psi_{k+1}\rangle = D(2\hat{H}_{scaled}|\psi_k\rangle - D|\psi_{k-1}\rangle), \quad k \geq 1 \tag{7}$$

where $|\psi_1\rangle = D\hat{H}_{scaled}|\psi_0\rangle$ and $|\psi_0\rangle = |\chi_i\rangle$. To impose outgoing boundary conditions, the following Gaussian shaped damping function D is applied at the grid edges:

$$D(x) = e^{-\alpha\left(\frac{x-x_a}{x_{\max}-x_a}\right)^n}, \tag{8}$$

where x=R and r_1, x_a is the starting point of the damping function. The scaled Hamiltonian is defined as $\hat{H}_{scaled} = (\hat{H} - H_+)/H_-$ to avoid the divergence of the Chebyshev propagator outside the range [-1,1]. The mean and half-width of the Hamiltonian were calculated from the spectral extrema $H_{\min}$ and $H_{\max}$ as $H_\pm = (H_{\max} \pm H_{\min})/2$. Since the initial wave packet is real, the Chebyshev iteration can be efficiently and accurately realized in real arithmetic.[46]

The action of the Hamiltonian is evaluated using in either the finite basis representation (FBR) and discrete variable representation (DVR).[47] The potential energy operator is diagonal in DVR, so the FBR wavefunction is transformed via one-dimensional pseudo spectral methods.[48] The flux through the dividing surface, $S = [r_1 = r_1^F]$, was calculated from the energy-dependent scattering wavefunction, which is obtained by Fourier transforming the wave packet at the dividing surface. The initial state-selected total reaction probability is computed as follows:[49]

Physical Chemistry Chemical Physics Accepted Manuscript

$$P^{J\varepsilon}_{\upsilon_0 j_0 \tau K_0}(E) = \frac{1}{2\pi\mu_1 |\, a_i(E)|^2\, (H^-)^2 \sin^2\theta} \times \mathrm{Im}\left\langle \sum_k (2-\delta_{k0}) e^{-ik\theta}\psi_k \middle| \sum_{k'} (2-\delta_{k'0}) e^{-ik'\theta}[\delta(r_1 - r_1^F)\frac{\partial}{\partial r_1}\psi_{k'}]\right\rangle. \quad (9)$$

where the Chebyshev angle $\theta = \arccos E_{scaled}$ is a non-linear mapping of the scaled energy.[50] The energy amplitude of the initial wave packet at the collision energy E is given by

$$a_i(E) = \langle \phi_{iE} | \chi_i \rangle, \quad (10)$$

where $|\phi_{iE}\rangle$ is the free scattering wavefunction. The choice of the analysis plane in the r_1 coordinate enables the calculation of the reaction flux into the HCl + OD arrangement channel.

In this study, we focus on the dynamics involving non-rotating reactant HOD, *i.e.*, j_0=0. Furthermore, the total reaction integral cross section (ICS) is calculated using the *J*-shifting approximation.[51] To this end, the partial wave contributions from non-vanishing J are all obtained from the J=0 probability by shifting the energy:

$$P^{J>0}(E) = P^{J=0}(E - \Delta E), \quad (11)$$

where $\Delta E = B^* J(J+1)$ with B^* as the rotational constant of the transition-state geometry.

The numerical parameters employed in the quantum calculations are given in Table I. The parameters were well tested to give converged results. The propagation was around 10000 steps for n_{OH} = 0,1 and 20000 steps for n_{OH} = 2,3,4.

II.C. Quasi-classical trajectory

Physical Chemistry Chemical Physics Accepted Manuscript

Standard QCT calculations were performed using VENUS.[52] The trajectories were initiated with a reactant separation of 8.0 Å, and terminated when products reached a separation of 15.0 Å, or when reactants are separated by 8.0 Å for non-reactive trajectories. The maximal impact parameter ($b_{\max}$) was determined using small batches of trajectories with trial values. The other scattering parameters (impact parameter, vibrational phases and spatial orientation of the initial reactants) were selected *via* a Monte Carlo approach. In particular, the angle variables for the HOD vibrational modes were selected randomly and then converted to the initial coordinates and momenta along with fixed action variables.[53] To account for anharmonicity corrections to the vibrational energies, the action variables were chosen to match the overtone energies, rather than from integers. During the propagation, the gradient of the PES was obtained numerically by a central-difference algorithm. The propagation time step was selected to be 0.05 fs. Energy conservation of the trajectories was found to be excellent with the chosen time step. Almost all trajectories conserved energy to within a chosen criteria (0.001 kcal/mol), which confirms the smoothness of the PES. Few exceptionally long trajectories, due apparently to trapping in the pre- and post-reaction complexes, were halted if the propagation time reached a pre-specified value (5.0 ps).

The total integral cross section (ICS) for the title reaction was computed according to the following formula:

$$\sigma_r\left(E_c\right) = \pi b_{\max}^2(E_c) P_r\left(E_c\right), \tag{12}$$

where the reaction probability P_r at the specified collision energy E_c is given by the ratio between the number of reactive trajectories (N_r) and total number of trajectories (N_{total}):

$$P_r\left(E_c\right) = N_r / N_{total}. \tag{13}$$

Physical Chemistry Chemical Physics Accepted Manuscript

The standard error is given by $\Delta = \sqrt{(N_{total} - N_r)/N_{total}N_r}$. Note that the impact parameter is sampled by $b=b_{max}R_n^{1/2}$, where R_n is a random number between 0 and 1.

Two types of binning were used for computing the product state distributions. The first one is the conventional histogram binning (HB), while the second was based on a Gaussian weighting function (GB).[54] The latter has been shown to better mimic the quantum distributions in some reactions.

III. Results

III.A. PIP-NN PES

Different NN architectures with two hidden layers were tested. For each architecture, 50 different training calculations were performed and the "early stopping" method[35] was used to avoid overfitting. As a compromise between efficiency and costs, a two-layer NN with 50 and 80 neurons in each layer was chosen, which has 5061 parameters. The training converged fast for all the fitting reported here, typically finishing within a few hundred steps. The final PIP-NN PES was chosen as the average of three best fits to minimize random errors. The RMSEs for the train/validation/test sets and maximum deviation of the three best PESs are 9.1/11.4/10.5/108.2, 9.1/11.4/12.7/111.1, and 7.8/12.2/12.2/143.3 meV, respectively. The final PES has a total RMSE of 8.4 meV, which is more accurate than the PIP fit, and a maximum deviation of 97.1 meV. The fitting errors of all the data points are shown in Fig. 2 as a function of energy.

Figure 3 presents a contour plot for the PIP-NN PES of the Cl+H_2O system as a function of the two coordinate r_1 and R with other Jacobi coordinates optimized. The reaction path for the title reaction involves a "late" barrier (indicated by a cross), featuring a bent transition state.[20, 26] There is a pre-reaction well resulted from a hemi-bonded Cl¨H_2O complex,[55] and a post-reaction

Physical Chemistry Chemical Physics Accepted Manuscript

well dominated by a hydrogen bond between the two products. The barrier of 20.5 kcal/mol and a reaction energy of 17.4 kcal/mol obtained at the MRCI+Q level[26] are well reproduced by the PES.

III.B Vibrational enhancement

Figure 4 shows the approximate QD ICS obtained by the *J*-shift method as a function of the collision energy (E_c) for the reaction Cl + HOD(n_{OH}=0-4) → HCl + OD. First, we note that the vibrational excitation in the OH stretching mode of the HOD reactant enhances the reactivity significantly for this late-barrier reaction, as expected. In the mean time, the energy threshold decreases with n_{OH} of the HOD reactant, eventually there is no threshold when $n_{OH}\geq 2$. Second, for n_{OH}=0 and 1, the ICS gradually increases with the collision energy, indicating the fact that the reaction is activated by the collision energy. This behavior is similar to that seen before for the Cl + H_2O reaction.[26] Unlike the F + H_2O reaction where the pre-reaction well enhances the reactivity by steering the trajectories to the transition state,[56] however, the pre-reaction well has little effect here, due apparently to the high "late" barrier in this endothermic reaction. For n_{OH}=2, on the other hand, there is a peak at E_c=0.08 eV and then the ICS decreases to a minimum at $E_c\approx$0.5eV, finally becomes relatively flat. For n_{OH}=3, the ICS firstly goes up to a peak at $E_c\approx$0.04eV and then decreases slowly. For n_{OH}=4, the ICS decreases monotonically with the collision energy. These trends are discussed in more detail below.

As a comparison, the QCT ICS for n_{OH}=4 is also calculated and it is consistent with the QD results. One can see that the trends are similar with the QD curve, although the QCT values are a little lower, which might be due to errors introduced by the *J*-shift approximation in the QD ICS. These results are consistent with the previous theoretical work based on not so accurate

Physical Chemistry Chemical Physics Accepted Manuscript

PESs and/or reduced dimensional models,[16-17] indicating the vibrational enhancement is quite robust, and insensitive to the model/PES used.

III.C Product state distribution

For the Cl + HOD(n_{OH}=4) → HCl + OD reaction at the experimental collision energy of 1390 cm^{-1},[8] the QCT results indicate that 99.7% of the trajectories break the O-H bond, which is in excellent agreement with the experimental estimate of 97.6%,[8] and with the previous QCT results of Kudla and Schatz of 99.9% at E_c=0.5eV based on a model PES.[16]

Figure 5 shows the calculated product vibrational state distributions of HCl and OD from the Cl + HOD(n_{OH}=4) → HCl + OD reaction at E_c=1390 cm^{-1}. As shown, the OD product is dominated by its ground vibrational state with a small population at the n=1 state, and a negligible population at the n=2 state. This is good agreement with the experimental populations of ≥95% in n=0, ≤5% in n=1 for OD.[8] In contrast, the HCl product is vibrationally hot, peaking at n=2. Unfortunately, there is no experimental data to compare with. Figure 6(a) compared the QCT and experimental rotational state distributions of OD (n_{OD}=0). One can see that they are in quantitatively agreement with each other, no matter if the HB or GB method is employed. In the same figure, rotational state distributions of the HCl product (Figures 6(b-d)) in three vibrational manifolds are displayed. Significant rotational excitations are apparent, but the extent of excitation decreases with the increasing vibrational quantum number. The HB and GB results are similar. Again, there is no experimental data to compare with.

IV. Discussion

Physical Chemistry Chemical Physics Accepted Manuscript

The theoretical results presented above clearly reproduced experimental results very well, particularly with respect to the bond selectivity. In addition, the theoretical calculations revealed more insights. First, the absolute cross section of the Cl + HOD(n_{OH}) → HCl + OD increases with n_{OH} in a dramatic fashion, cumulating with a very large 7.0 Å^2 for n_{OH}=4. Although there has been no experimentally measured cross section for this reaction, exceedingly large cross sections have been reported for a very similar reaction: H + H_2O(n=4) → H_2 + OH.[57] This large cross section is important to compensate the small excitation efficiency in the overtone pumping, presumably responsible for making the experiment possible. Second, the excitation functions for different levels of OH vibrational excitation in the HOD reactant show very different behaviors. For null and low vibrational excitations, the ICS increases with the collision energy, as expected for an activated reaction. For highly vibrational excited HOD, however, the ICS becomes a monotonically decaying function of the collision energy with no threshold. This signals a change of reaction mechanism. Indeed, the total vibrational energy above the zero point energy in HOD(n_{OH}=4) is 39.5 kcal/mol, much higher than the reaction barrier. Interestingly, the corresponding ICS behaves much like that of a barrierless capture reaction often seen in complex-forming reactions.[58-59] As pointed out by Lendvay and coworkers,[25] such reactions with highly vibrationally excited reactants do not follow the conventional minimum energy pathway via the transition state and the effective interaction potential becomes attractive for the stretched HOD. This is borne out in Fig. 7 where the potential energy curves between the two reactants are displayed for different r_1 (essentially the O-H bond distance) values. The change of reaction mechanism is further supported by the product angular distributions, i.e., differential cross sections (DCS), and the opacity function displayed in Fig. 8. As shown, the DCS for the Cl + HOD(n_{OH}=4) reaction is forward dominated. This is in sharp contrast to the backward angular

Physical Chemistry Chemical Physics Accepted Manuscript

distribution for the Cl + H_2O reaction with the reactant in its ro-vibrational ground state,[26] which is indicative of a direct rebound mechanism. In addition, the opacity function in the same figure indicates that the title reaction is most probable at the impact parameter of *b*=2 Å, about twice of that in the Cl reaction with ground vibrational state of H_2O.[26]

The enhancement of the bond-selective reactivity in this reaction can be explained by our recently proposed Sudden Vector Projection (SVP) model.[29-30] The SVP model argues that the intramolecular vibrational energy redistribution (IVR) of the reactants is often much slower than the collision time. As a result, such a reaction can be treated in the sudden limit. Furthermore, the SVP model attributes the efficacy of a reactant mode in promoting the reaction to its coupling with the reaction coordinate at the transition state, which is quantified by the overlap between the reactant normal mode ($\vec{Q}_i$) and reaction coordinate vectors ($\vec{Q}_{RC}$): $P_i = \vec{Q}_i \cdot \vec{Q}_{RC} \in [0,1]$. It has been shown that for many gas phase and gas-surface reactions, the SVP model appears to be quite good for predicting the effects of reactant vibrational modes.[33] The SVP model can be considered as a generalization of Polanyi's Rules,[15] which is based on the location of the barrier. For convenience, the SVP values are listed in Table II. It is clear that the OH vibrational vector of HOD is the only reactant mode that is well aligned with the reaction coordinate, suggesting that they are strongly coupled, thus rationalizing the vibrationally enhanced bond selectivity.

In addition to the bond selectivity, our theoretical calculations also yield product state distributions. The agreement with the available experimental data is quite satisfactory. Interestingly, our SVP model can also be used to predict the energy disposal in the product channel if they are considered as mode specificity for the reverse reaction.[29-30] As indicated by the SVP values in Table II, HCl is predicted to be both vibrationally and rotationally excited, while OD is essentially a spectator bond during the reaction, with small SVP values in

Physical Chemistry Chemical Physics Accepted Manuscript

vibrational and rotational modes of OD. Some energy is also predicted to be disposed in the translational coordinate. These predictions by the SVP model are borne out by our QCT results.

V. Conclusions

The reaction dynamics of the bond selective reaction Cl + HOD(n_{OH}) → HCl + OD has been investigated using full-dimensional QD and QCT approaches on a newly constructed PIP-NN PES. The QCT results agree well with the QD counterparts except for some quantitative differences, suggesting that quantum effects have a small impact on the reaction dynamics. In particular, the effects of vibrationally exciting the local OH(n_{OH}=0, 1, 2, 3, and 4) mode of the HOD reactant on the reactivity have been studied. The main conclusions are:

1) The preferred bond session always involves the vibrationally excited O-H bond, in excellent agreement with experimental observations. The near unity experimental OD branching ratio for the Cl + HOD(n_{OH}=4) reaction is satisfactorily reproduced.

2) The bond selective reactivity increases significantly with the OH vibrational excitation in the HOD reactant.

3) The excitation function changes its energy dependence with the reactant OH vibrational excitation, signaling a change of reaction mechanism. For the highly excited HOD reactant, the effective approaching potential becomes attractive, leading to a capture-like behavior of the excitation function. The change of mechanism is also supported by the opacity function and differential cross section.

4) The HCl product is found to be rotationally and vibrationally excited, while the OD co-product is internally cold, in good agreement with available experimental data.

Physical Chemistry Chemical Physics Accepted Manuscript

5) All these results, namely bond selectivity, vibrational enhancement, and product energy disposal, can be rationalized by the SVP model. Essentially, the reaction coordinate at the corresponding transition state is strongly coupled with the OH vibration in the HOD reactant, and with the HCl rotational and vibrational coordinates.

The reproduction of available experimental data strongly supports the accuracy of the PES. Importantly, the theoretical results presented here shed further light on bond-selective chemistry of gas phase bimolecular reactions with vibrationally excited reactants. Some of the conclusions obtained in the current study are probably not restricted to the title reaction. However, more studies are needed to confirm their general validity.

Acknowledgements: This work was supported by Department of Energy (DE-FG02-05ER15694 to HG), and the Hundred-Talent Foundation of Chongqing University (project no. 022000530001 to JL).

Physical Chemistry Chemical Physics Accepted Manuscript

Table I. Numerical parameters used in the wave packet calculations. (Atomic units are used unless stated otherwise.)

	Cl + HOD
Grid/basis range and size:	$R \in [2.0, 18.0]$, $N_R^{total}=280$, $N_R^{int}=90$ $N_{r_1}^{int}=47$, $N_{r_1}^{asymp}=9$ $N_{r_2}=6$ $j_{1\max}=62$, $j_{2\max}=28$
Initial wave packet:	$R_0=15.5$, $\delta=0.35$, $E_i=0.15$ eV
Absorbing potential:	$R_a=16.0$, $\alpha_R=0.05$, $n_R=1.5$ $r_{1a}=4.2$, $\alpha_{r_1}=0.05$, $n_{r_1}=1.5$
Flux position:	$r_1^F=4.0$

Physical Chemistry Chemical Physics Accepted Manuscript

Table II. SVP values for the Cl + HOD → HCl + OD reaction.

Species	Mode	SVP
Cl+HOD	OH stretch	0.99
	OD stretch	0.09
	Bend	0.06
	Rotation	0.01
	Translation	0.07
HCl+OD	HCl vibration	0.75
	HCl rotation	0.25
	OD vibration	0.01
	OD rotation	0.09
	Translation	0.21

Physical Chemistry Chemical Physics Accepted Manuscript

References:

1 R. N. Zare, Science **279**, 1875 (1998).
2 F. F. Crim, Acc. Chem. Res. **32**, 877 (1999).
3 G. Czakó and J. M. Bowman, J. Phys. Chem. A **118**, 2839 (2014).
4 F. F. Crim, J. Phys. Chem. **100**, 12725 (1996).
5 D. J. Nesbitt and R. W. Field, J. Phys. Chem. **100**, 12735 (1996).
6 S. Yan, Y.-T. Wu and K. Liu, Proc. Natl. Acad. Sci. USA **105**, 12667 (2008).
7 A. Sinha, J. D. Thoemke and F. F. Crim, J. Chem. Phys. **96**, 372 (1992).
8 J. D. Thoemke, J. M. Pfeiffer, R. B. Metz and F. F. Crim, J. Phys. Chem. **99**, 13748 (1995).
9 A. Sinha, M. C. Hsiao and F. F. Crim, J. Chem. Phys. **92**, 6333 (1990).
10 A. Sinha, M. C. Hsiao and F. F. Crim, J. Chem. Phys. **94**, 4928 (1991).
11 M. C. Hsiao, A. Sinha and F. F. Crim, J. Phys. Chem. **95**, 8263 (1991).
12 M. J. Bronikowski, W. R. Simpson, B. Girard and R. N. Zare, J. Chem. Phys. **95**, 8647 (1991).
13 M. J. Bronikowski, W. R. Simpson and R. N. Zare, J. Phys. Chem. **97**, 2194 (1993).
14 R. B. Metz, J. D. Thoemke, J. M. Pfeiffer and F. F. Crim, J. Chem. Phys. **99**, 1744 (1993).
15 J. C. Polanyi, Acc. Chem. Res. **5**, 161 (1972).
16 K. Kudla and G. C. Schatz, Chem. Phys. **175**, 71 (1993).
17 G. Nyman and D. C. Clary, J. Chem. Phys. **100**, 3556 (1994).
18 J. R. Fair, D. Schaefer, R. Kosloff and D. J. Nesbitt, J. Chem. Phys. **116**, 1406 (2002).
19 N. Rougeau, Phys. Chem. Chem. Phys. **9**, 2113 (2007).
20 Y. Guo, M. Zhang, Y. Xie and H. F. Schaefer III, J. Chem. Phys. **139**, 041101 (2013).
21 D. C. Clary, Chem. Phys. Lett. **192**, 34 (1992).
22 K. Kudla and G. C. Schatz, Chem. Phys. Lett. **193**, 507 (1992).
23 D. H. Zhang and J. C. Light, J. Chem. Soc. Faraday Trans. **93**, 691 (1997).
24 D. Troya, M. Gonzalez and G. C. Schatz, J. Chem. Phys. **114**, 8397 (2001).
25 E. Bene, G. Lendvay and G. Pota, J. Phys. Chem. A **109**, 8336 (2005).
26 J. Li, R. Dawes and H. Guo, J. Chem. Phys. **139**, 074302 (2013).
27 B. Jiang and H. Guo, J. Chem. Phys. **139**, 054112 (2013).
28 J. Li, B. Jiang and H. Guo, J. Chem. Phys. **139**, 204103 (2013).
29 B. Jiang and H. Guo, J. Am. Chem. Soc. **135**, 15251 (2013).
30 B. Jiang and H. Guo, J. Chem. Phys. **138**, 234104 (2013).
31 B. Jiang, J. Li and H. Guo, J. Chem. Phys. **140**, 034112 (2014).
32 J. Li and H. Guo, J. Phys. Chem. A **118**, 2419 (2014).
33 H. Guo and B. Jiang, Acc. Chem. Res. **in press (DOI: 10.1021/ar500350f)** (2014).
34 B. J. Braams and J. M. Bowman, Int. Rev. Phys. Chem. **28**, 577 (2009).
35 L. M. Raff, R. Komanduri, M. Hagan and S. T. S. Bukkapatnam, *Neural Networks in Chemical Reaction Dynamics*. (Oxford University Press, Oxford, 2012).
36 Z. Xie and J. M. Bowman, J. Chem. Theo. Comp. **6**, 26 (2010).
37 D. H. Zhang and J. C. Light, J. Chem. Phys. **104**, 4544 (1996).
38 D. H. Zhang and J. Z. H. Zhang, J. Chem. Phys. **101**, 1146 (1994).
39 R. N. Zare, *Angular Momentum*. (Wiley, New York, 1988).
40 B. Jiang, D. Xie and H. Guo, J. Chem. Phys. **135**, 084112 (2011).
41 J. Ma, J. Li and H. Guo, J. Phys. Chem. Lett. **3**, 2482 (2012).
42 B. Jiang and H. Guo, J. Chem. Phys. **139**, 224310 (2013).
43 S. K. Gray and G. G. Balint-Kurti, J. Chem. Phys. **108**, 950 (1998).
44 V. A. Mandelshtam and H. S. Taylor, J. Chem. Phys. **103**, 2903 (1995).
45 R. Chen and H. Guo, J. Chem. Phys. **105**, 3569 (1996).

Physical Chemistry Chemical Physics Accepted Manuscript

46 S. K. Gray, in *Advances in Molecular Vibrations and Collision Dynamics* (JAL, 1991).
47 J. C. Light and T. Carrington Jr., Adv. Chem. Phys. **114**, 263 (2000).
48 G. C. Corey, J. W. Tromp and D. Lemoine, in *Numerical Grid Methods and Their Applications to Schroedinger's Equation*, edited by C. Cerjan (Kluwer, Dordrecht, 1993), pp. 1-23.
49 S. Y. Lin and H. Guo, J. Chem. Phys. **119**, 11602 (2003).
50 R. Chen and H. Guo, J. Chem. Phys. **108**, 6068 (1998).
51 J. M. Bowman, J. Phys. Chem. **95**, 4960 (1991).
52 W. L. Hase, R. J. Duchovic, X. Hu, A. Komornicki, K. F. Lim, D.-H. Lu, G. H. Peslherbe, K. N. Swamy, S. R. V. Linde, A. Varandas, H. Wang and R. J. Wolf, Quantum Chemistry Program Exchange Bulletin **16**, 671 (1996).
53 W. L. Hase, in *Encyclopedia of Computational Chemistry*, edited by N. L. Alinger (Wiley, New York, 1998), Vol. 1, pp. 399-402.
54 L. Bonnet, Int. Rev. Phys. Chem. **32**, 171 (2013).
55 J. Li, Y. Li and H. Guo, J. Chem. Phys. **138**, 141102 (2013).
56 J. Li, B. Jiang and H. Guo, Chem. Sci. **4**, 629 (2013).
57 G. Hawthorne, P. Sharkey and I. W. M. Smith, J. Chem. Phys. **108**, 4693 (1998).
58 D. C. Clary, Mole. Phys. **53**, 3 (1984).
59 H. Guo, Int. Rev. Phys. Chem. **31**, 1 (2012).

Physical Chemistry Chemical Physics Accepted Manuscript

Figure Captions:

Figure 1. The six-dimensional Jacobi coordinates for the Cl + HOD reaction.

Figure 2. Fitting error (E_{fit}-$E_{abinito}$) using the PIP-NN method as a function of the *ab initio* energy.

Figure 3. Contour plot for the PIP-NN PES along the reaction coordinate r_1 and R distances (both in bohr) with all other Jacobi coordinates optimized. Energies are in kcal/mol relative to the reactants. The transition state is indicated by the cross (×).

Figure 4. *J*-shifting QD ICS for the reaction Cl + HOD(n_{OH}=0, 1,2,3, and 4) → HCl + OD. The QCT ICS for n_{OH}=4 is also compared in (*d*). Note the vastly different scales of the panels.

Figure 5. Normalized QCT vibrational state distributions of the HCl and OD product from the reaction Cl + HOD(n_{OH}=4) → HCl + OD and E_c=1390cm^{-1}.

Figure 6. Normalized QCT rotational quantum state distributions of vibrationally ground state OD((a)) and of the product HCl at different vibrational states (n_{HCl}=1, 2, and 3, (b), (c), and (d)). The experimental results are adopted from Ref. [8].

Figure 7. (*a*) Potential energy of HOD along the OH bond when the OD and bond angle are at equilibrium geometry. The OH eigenstates are also shown. (*b*) Potential energy along R with r_1 at different values and other Jacobi coordinates fixed at the transition state geometry.

Figure 8. (*a*) Product angular distributions and (*b*) opacity function $P(b)$ for Cl + HOD(n_{OH}=4) → HCl + OD at E_c=1390 cm^{-1} calculated using the QCT method.

Physical Chemistry Chemical Physics Accepted Manuscript

Figure 1.

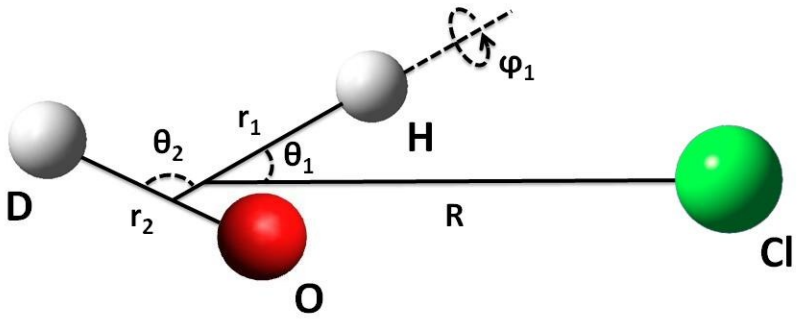

Physical Chemistry Chemical Physics Accepted Manuscript

Figure 2.

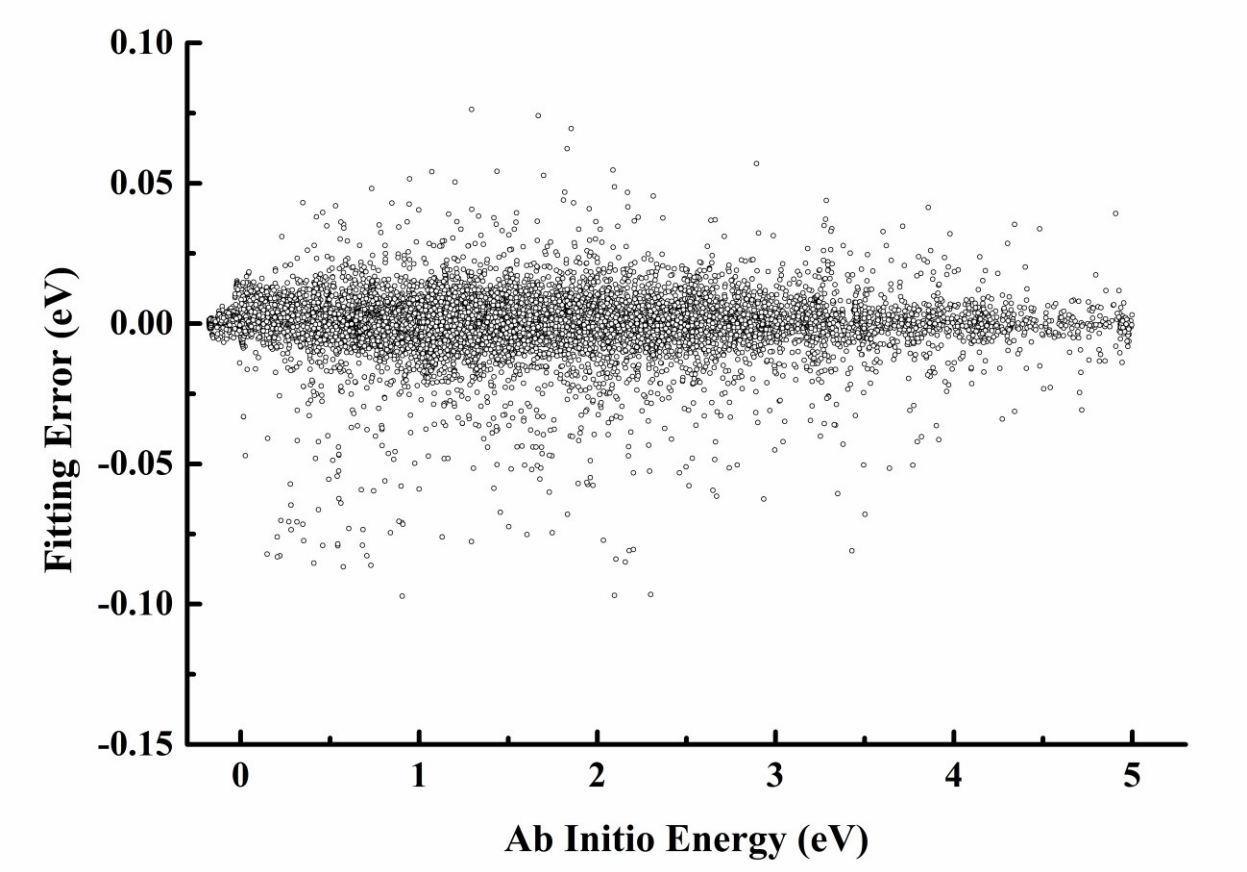

Physical Chemistry Chemical Physics Accepted Manuscript

Figure 3.

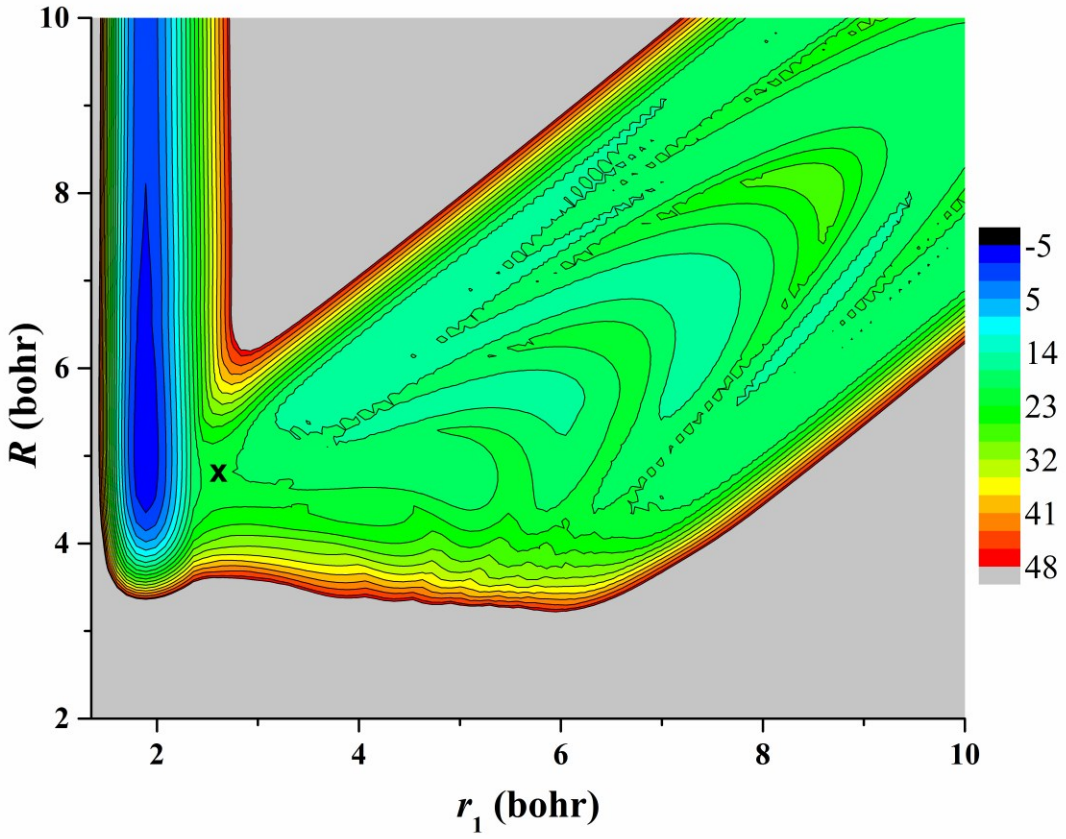

Physical Chemistry Chemical Physics Accepted Manuscript

Figure 4.

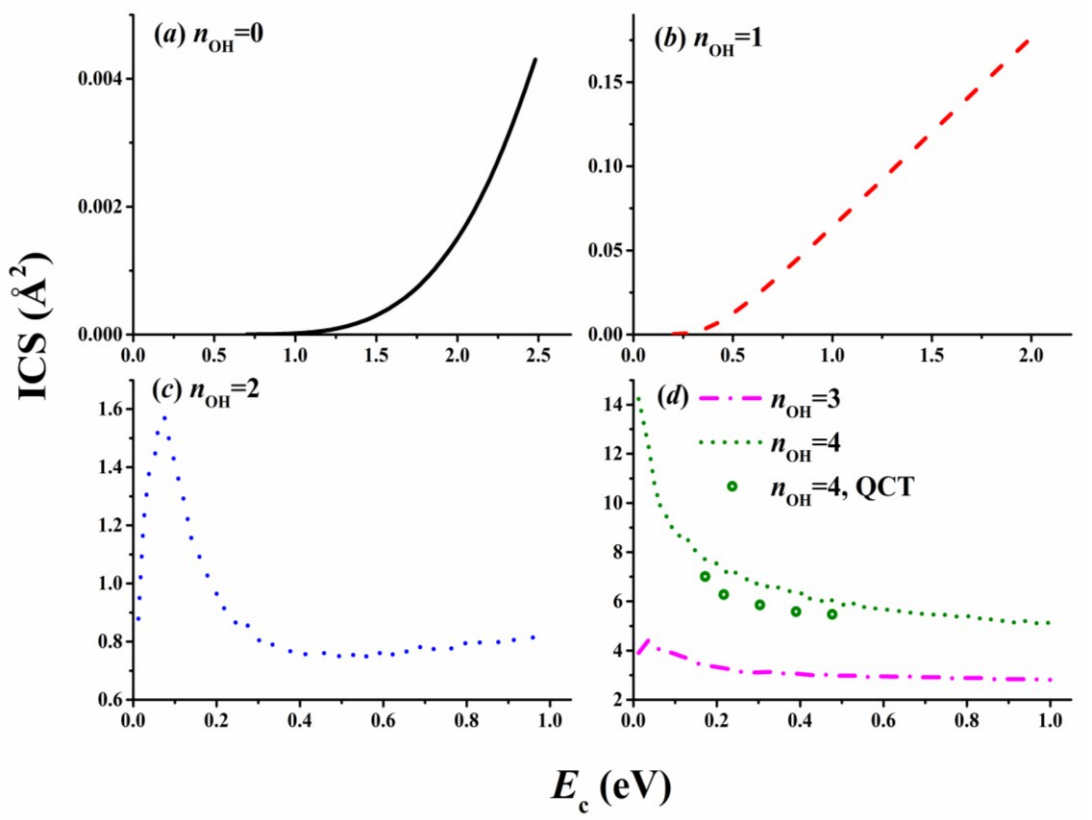

Physical Chemistry Chemical Physics Accepted Manuscript

Figure 5.

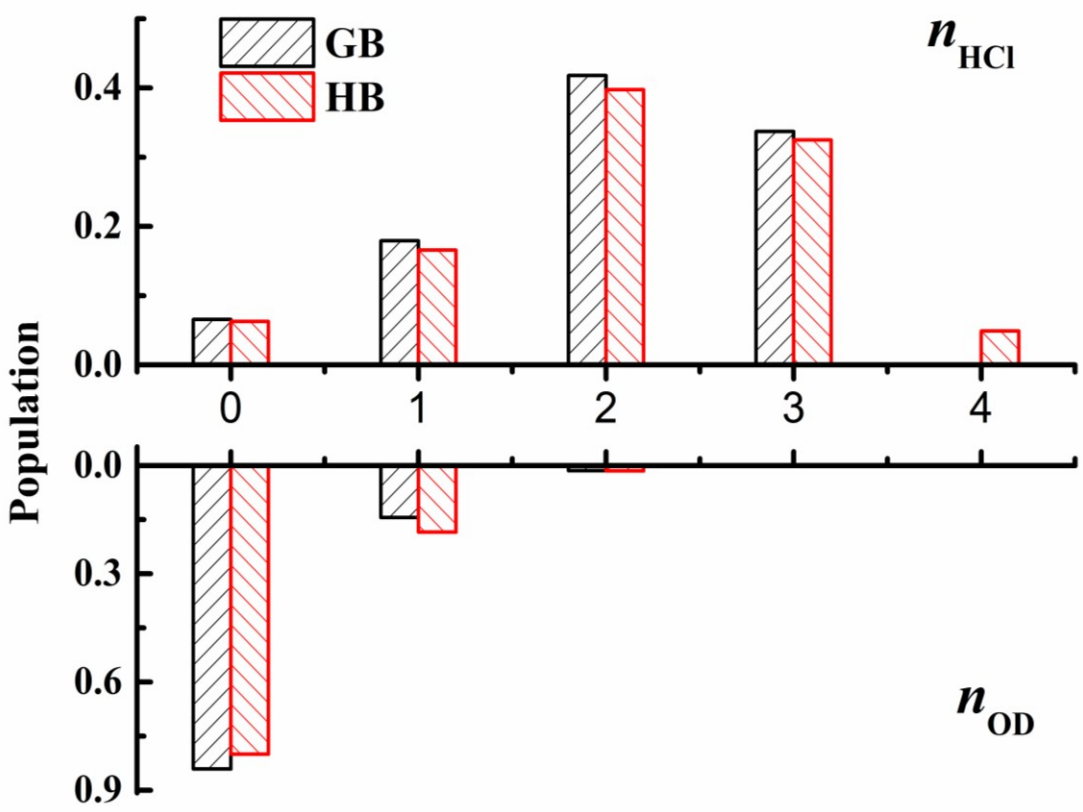

Physical Chemistry Chemical Physics Accepted Manuscript

Figure 6.

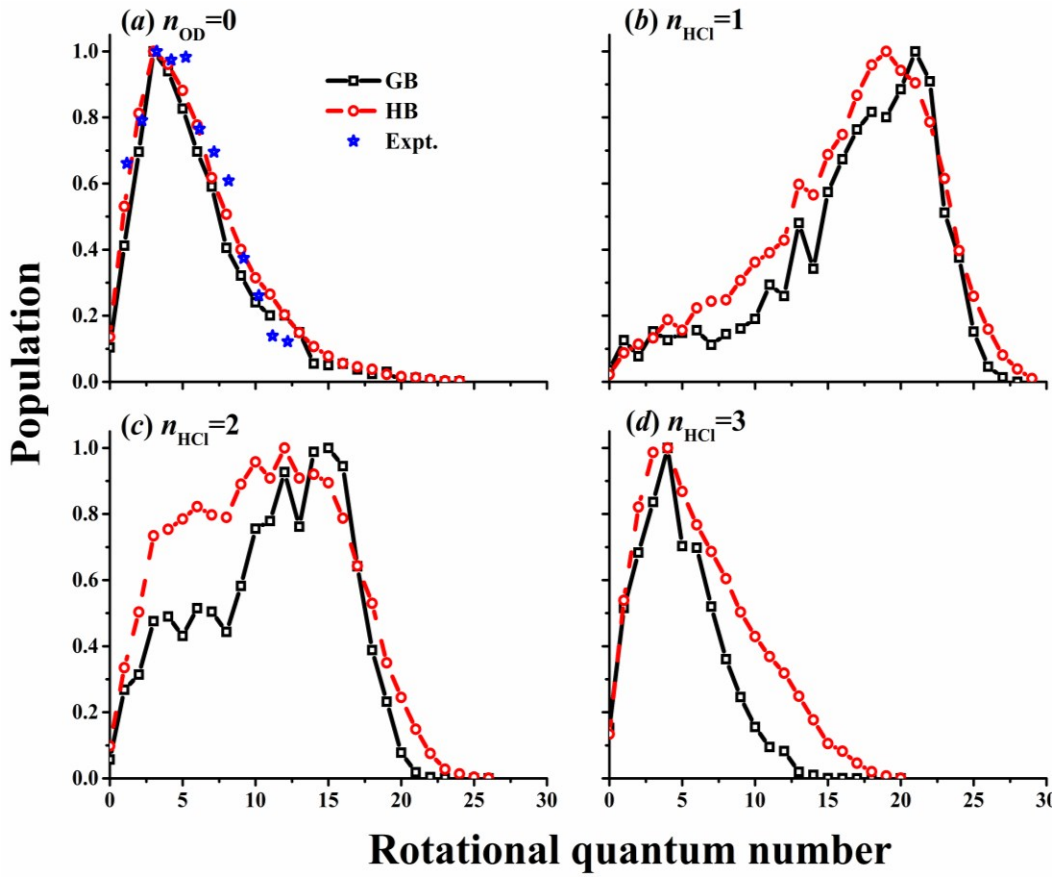

Physical Chemistry Chemical Physics Accepted Manuscript

Figure 7.

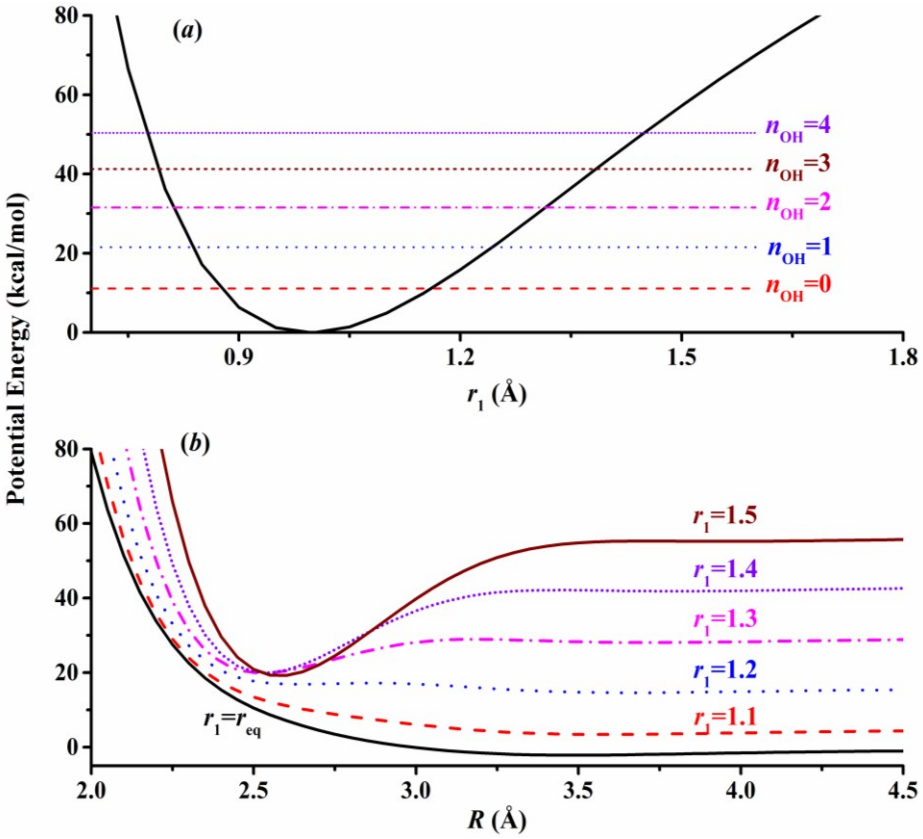

Physical Chemistry Chemical Physics Accepted Manuscript

Figure 8.

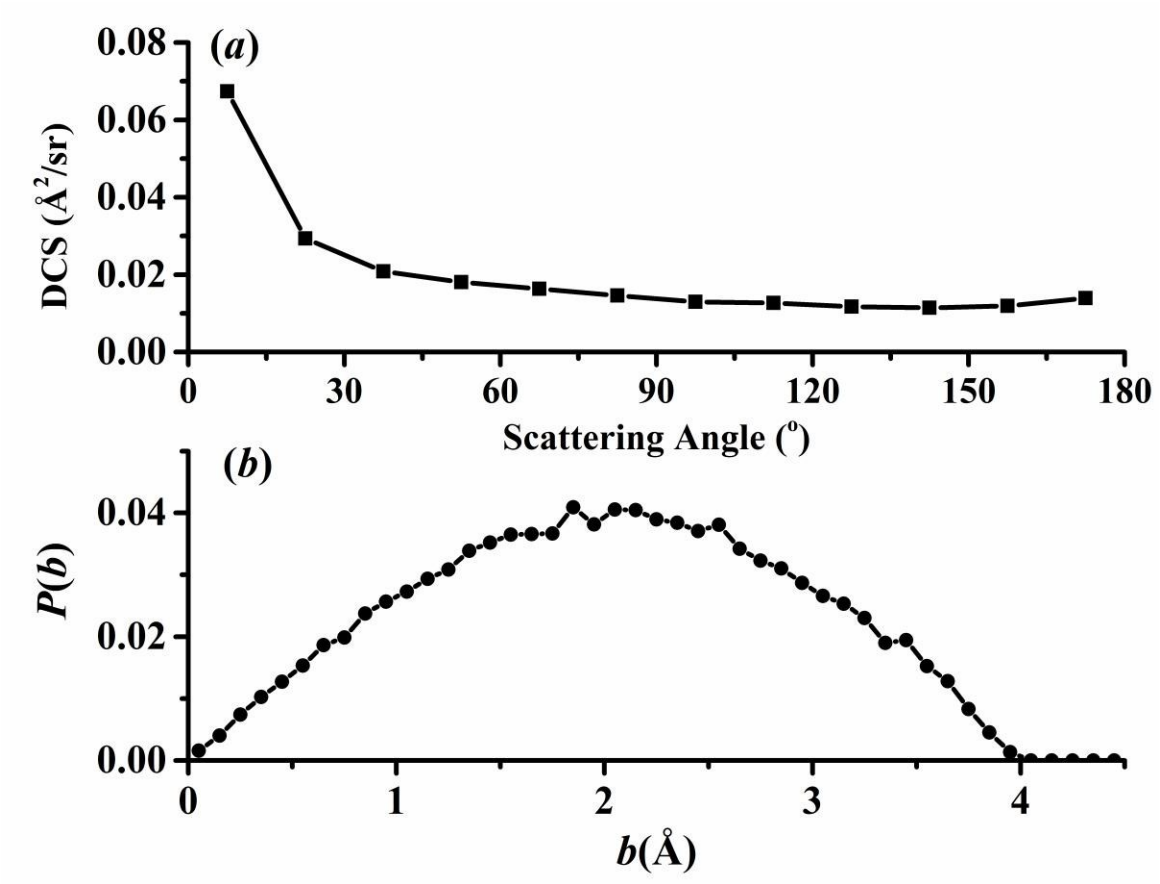

Physical Chemistry Chemical Physics Accepted Manuscript

TOC graphic

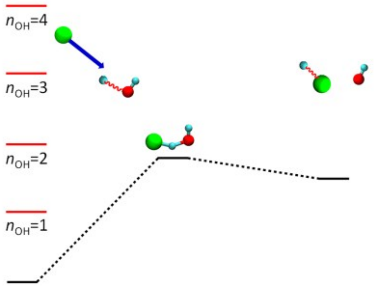

Theoretical study of the title reaction reveals strong bond selectivity, vibrational enhancement, and unique product distributions, in agreement with experiment.

Physical Chemistry Chemical Physics Accepted Manuscript